ARTICLE

Metal Nanoparticle Wires Formed by an Integrated Nanomolding–Chemical Assembly Process: Fabrication and Properties

Xuexin Duan,[†,⊥,¶] Myoung-Hwan Park,[§,¶] Yiping Zhao,[†,‡] Erwin Berenschot,[‡] Zheyao Wang,[⊥] David N. Reinhoudt,[†] Vincent M. Rotello,[§,*] and Jurriaan Huskens[†,*]

[†]Molecular Nanofabrication Group, [‡]Transducers Science and Technology Group, MESA+ Institute for Nanotechnology, University of Twente, P.O. Box 217, 7500 AE Enschede, The Netherlands, [§]Department of Chemistry, University of Massachusetts, 710 North Pleasant Street, Amherst, Massachusetts 01003, United States, and [⊥]Institute of Microelectronics of Tsinghua University 100084, Beijing, China. [¶]These authors contributed equally to this work.

ABSTRACT We report here the use of nanomolding in capillaries (NAMIC) coupled with dithiocarbamate (DTC) chemistry to fabricate sub-50 nm quasi-1D arrays of 3.5 nm core gold nanoparticles (Au NPs) over large areas. Owing to chemical immobilization *via* the DTC bond, the patterned NP systems are stable in water and organic solvents, thus allowing the surface modification of the patterned Au NP arrays through thiol chemistry and further orthogonal binding of proteins. The electrical properties of these patterned Au NP wires have also been studied. Our results show that NAMIC combined with surface chemistry is a simple but powerful tool to create metal NP arrays that can potentially be applied to fabricate nanoelectronic or biosensing devices.

KEYWORDS: soft lithography · nanomolding in capillaries · nanoparticles · nanoparticle wires · conductance

Nanoparticles (NPs) feature unique electronic, photonic, and magnetic properties that make them promising candidates as building blocks for the next generation of nanodevices.[1−5] One of the keys to the use of NPs in future technologies is their controllable and precise assembly into ordered low-dimensional structures.[6] During the past few years, a range of techniques for spatial ordering of two- and three-dimensional NP arrays have been developed.[7−10] Along with two- or three-dimensional NP arrays, NPs in one-dimensional (1D) (wire-type) or quasi 1D arrays are of particular interest, both theoretically and experimentally[11−17] because of their value in understanding fundamental problems such as localization, hopping, and the formation of the energy bands in discrete but coupled systems. However, assembling 1D NP arrays is challenging due to the difficulty in obtaining continuously connected 1D superstructures over longer length scales. To circumvent the difficulty in constructing 1D structures from isotropic NPs, most previous studies have focused on assembling NPs on 1D templates such as DNA,[18,19] nanowires,[20] 1D-structured substrates,[21,22] templates fabricated by advanced lithography,[12,23−25] *etc*. Although template assembly is effective, direct patterning methods of 1D NP arrays on planar substrates would enable facile production in large quantity and low cost with high throughput.

We have recently developed a soft lithographical approach,[26] nanomolding in capillaries (NAMIC), to pattern functional materials on the sub-100 nm scale.[27] NAMIC uses a hybrid stamp with harder, more well-defined features that is fabricated by nanoimprint lithography (NIL) on flat polydimethylsiloxane (PDMS) as the nanomold, thus allowing large areas (over several cm^2) patterning of NP arrays in one-step with relatively low cost. Here, we report the use of NAMIC to pattern small gold nanoparticles (3.5 nm, core diameter) into stable 1D NP arrays through the use of dithiocarbamate (DTC)-based surface chemistry.[28−30] The covalent linking of Au NPs on the substrate through DTC bond formation provides 1D arrays having a uniform layer of NPs on the surface with high stability to organic solvents and water. These NP arrays provide systems for studying the electrical properties of the 1D NP, wire-like arrays. Moreover, owing to the robust chemical immobilization, the patterned Au NPs can be further modified through functional thiols to bind proteins that potentially can be used for biosensing applications.

*Address correspondence to j.huskens@utwente.nl, rotello@chem.umass.edu.

Received for review September 20, 2010 and accepted November 10, 2010.

Published online November 17, 2010. 10.1021/nn102463r

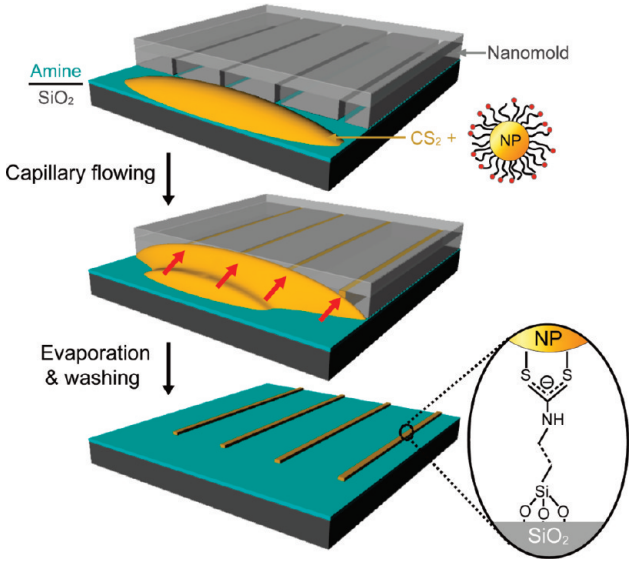

Scheme 1. Process scheme for the formation of 1D Au NP arrays using NAMIC coupled with DTC chemistry to pattern Au NPs into 1D arrays

RESULTS AND DISCUSSION

Scheme 1 shows a schematic outline of the NAMIC process combined with DTC chemistry to pattern Au NPs. First, an amine-functionalized self-assembled monolayer (SAM) of *N*-[3-(trimethoxysilyl)propyl]ethylenediamine (TPEDA) was prepared on a silicon oxide surface. The hybrid PDMS nanomold was fabricated by NIL with a thin film of thermal resist on a composite flat PDMS substrate according to a previously published procedure.[31] Polymer nanogrooves of 30 or 100 ± 5 nm separated by 4 μm were formed on the PDMS surface. A typical length of the PDMS nanomold was 0.5−1.5 cm, and the width of the mold was 0.5−2 cm. The mold can contain about 1250−5000 parallel channels. Then, the PDMS nanomold was soft bonded to the amine-functionalized SiO_2 substrates to form a parallel array of nanochannels. The channels were then filled with a solution containing CS_2 and Au−TOH NPs (~3.5 nm core diameter, coated with TOH (monohydroxy(1-mercaptoundecyl)-tetraethylene glycol)) ligands. Driven by capillary forces, the CS_2 and Au−TOH NP solution fills the nanochannels. The primary amine on the surface is converted to DTC by reaction with CS_2 that then displaces some TOH ligands on the Au NPs, binding the NPs onto the surface within the confinement of the nanochannels. The process is simple, clean, and reliable and is based on water/alcohol solutions, providing eco-friendly fabrication. After evaporation of the solvent and detachment of the mold, the Au NPs are deposited on the substrate. A short oxygen plasma step was applied to remove the organic residues due to the bonding of the PDMS mold. This may remove to some extent also the organic shell at the top of the particles at the structures. The physisorbed NPs can be rinsed away by solvent, thus

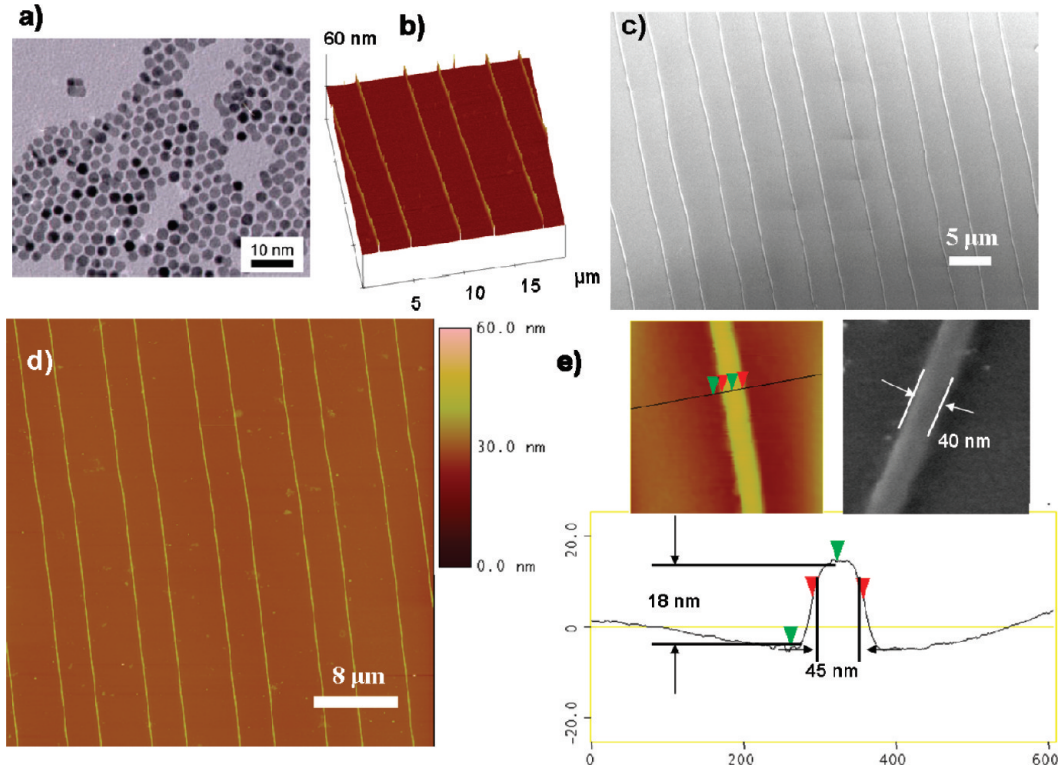

Figure 1. (a) TEM image of the Au NPs used in the assembly step. 3D AFM (b), SEM (c), AFM height images (d), and section analysis (e) of Au NP patterns fabricated using a 30 nm × 100 nm (*w* × *h*) mold on Si/SiO_2 after O_2 plasma by NAMIC combined with DTC chemistry.

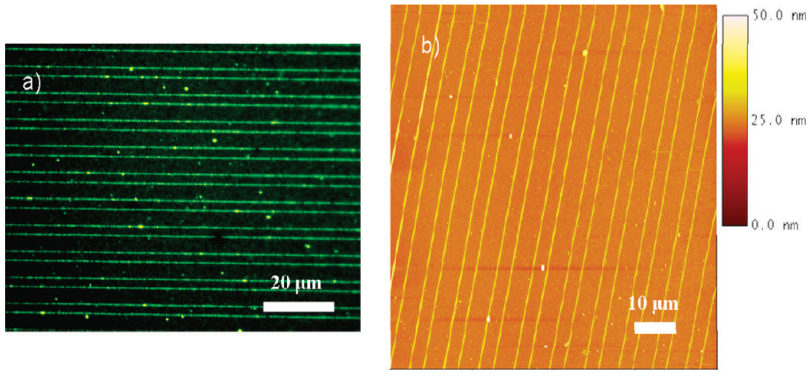

Figure 2. (a) Fluorescence micrograph of patterned QD-TOH NPs and (b) AFM height image of patterned FePt−TOH NPs on Si/SiO_2 by NAMIC combined with DTC chemistry using a 100 nm × 100 nm (*w* × *h*) PDMS nanomold.

leaving a uniform array of 1D Au NP lines on the substrate.

Figure 1 a shows a representative transmission electron microscopy (TEM) image of the Au NPs used in the assembly step. Measured from the TEM image, the Au NPs have an overall average diameter of ~7 nm (metal core + the ligands size). Figure 1b−e shows the scanning electron microscope (SEM) and atomic force microscopy (AFM) height images of the Au NP patterns which were fabricated through a 30 nm × 100 nm (*w* × *h*) PDMS nanomold onto an amine-functionalized Si/SiO_2 substrate.

As observed in the AFM and SEM images, after NAMIC and rinsing with solvent, the Au NPs formed continuous nanolines over large areas without obvious defects. The nanolines have an average width of 40 ± 5 nm that is somewhat larger than the width of the PDMS nanomold (30 nm). This is probably due to the short exposure of oxygen plasma to the PDMS nanomold before the binding. The height of the Au NP arrays is 18 ± 2 nm measured from AFM line scans, and no change was seen upon further sonication in ethanol. The height of the Au NP patterns (~18 nm) corresponds to ~2 to 3 layers of the Au NPs, probably owing to the closed packing of the Au NPs during the solvent evaporation within the nanochannels, while the width corresponds to about 5−6 NPs.

A control experiment was done by deposition of Au−TOH NPs in the absence of CS_2 under the same conditions through NAMIC. After mold detachment and rinsing, we observed that the Au NPs formed broken lines on the substrates due to the rinsing with ethanol (see Supporting Information). Upon further sonication, the patterned Au NPs could be completely removed from the substrate. It proves that, in the absence of CS_2, the Au−TOH NPs were only physisorbed on the substrate and that DTC bond formation is essential to achieve stable NP patterns.

The NAMIC approach combined with DTC chemistry can be applied to different types of NPs since CS_2-mediated ligand exchange also works for NP systems featuring other thiophilic core materials. To demonstrate this versatility, we have patterned both core−shell CdSe−ZnS quantum dots (QD-TOH, 2.8 nm) and superparamagnetic FePt NPs (FePt−TOH, 2.4 nm) under the same conditions. Figure 2 shows a representative fluorescence micrograph and AFM image of both patterned NP arrays.

To demonstrate the robustness of the structures, as well as fabrication of contacts, a substrate with prepatterned Au NP lines was patterned by NAMIC again to create a second set of parallel lines to achieve cross patterning. Owing to the robust interactions by the DTC bond, the first Au NP lines are quite stable upon contacting with the second PDMS nanomold. Figure 3a shows the process of making crossed lines by two sequential depositions. The first set of parallel Au NP lines was deposited on an amine-functionalized silicon substrate by NAMIC combined with DTC bond formation (Scheme 1). Upon PDMS demolding and rinsing with ethanol and further cleaning by O_2 plasma, the TPEDA layer was regenerated from its solutions on the silicon dioxide surface. The substrate was then rotated by 90° and contacted to another PDMS nanomold, and then Au−TOH NPs were deposited again under the same conditions. The second set of Au lines overlaps with the first one, forming a grid pattern (Figure 3b−e).

As clearly seen from the SEM and AFM images (Figure 3b−e), the Au NPs formed grid patterns over large areas. Nanolines overlapped one another with uniform width (100 or 40 ± 5 nm) which compares well with the dimensions of the PDMS nanomold. The height of the lines is 18 ± 2 nm except at the junctions (~30 nm). This cross patterning through the NAMIC approach could enable an ordered orthogonal assembly onto the substrate if a second type of NPs is used, one that provides a useful device platform for investigating the interactions between two different sets of NPs at the junctions of such grid patterns.

Owing to the stable chemical immobilization *via* the robust DTC bond that is actually stronger than an Au−thiol bond,[29,30] the patterned Au NP lines are stable in water and organic solvents, allowing further surface modification of the Au lines through functionalized thiols. As an example, a positively charged hydrophilic thiol ligand TTMA (HS-C_{11}-tetra(ethylene glycol)-NMe_3^+) was used to modify the surface of the Au nanolines by incubating the patterned Au nanolines in the TTMA ethanol solution (0.1 μM) for 8 h. The samples were then thoroughly washed with ethanol to achieve arrays of TTMA monolayer-functionalized Au nanolines (Au−TTMA). Due to the positive charges provided by the TTMA ligands, Au−TTMA can be further used for the specific binding of negatively charged materials by electrostatic assembly (Figure 4a). Negatively charged, fluorescein isothiocyanate-labeled bovine serum albu-

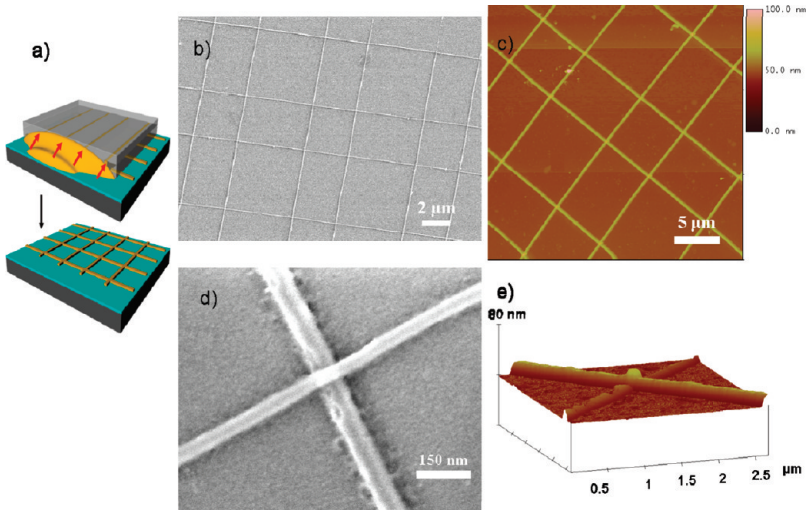

Figure 3. (a) Schematic diagram illustrating grid patterns obtained by two sequential NAMIC steps. SEM (b) and AFM (c) images of Au−TOH NPs grid patterns fabricated on Si/SiO_2 by NAMIC coupled with DTC chemistry using the 100 nm × 100 nm (w × h) mold twice. SEM (d) and 3D AFM (e) images of the Au−TOH NP patterns by NAMIC combined with DTC chemistry using the 100 nm × 100 nm (w × h) mold first and the 30 nm × 100 nm mold second.

min (FITC-BSA) was deposited onto the Au−TTMA from an aqueous solution. After rinsing with water, the samples were imaged by fluorescence microscopy and AFM (Figure 4b−e).

From the fluorescence images (Figure 4b,c) taken after surface modification of the Au NP nanolines by TTMA and the postdeposition of FITC-BSA, continuous fluorescence line patterns were observed over large areas on the substrate, thus indicating the successful deposition of FITC-BSA selectively on the positively charged Au−TTMA nanolines. Measuring from the AFM height images of the patterned Au nanolines before and after functionalization by TTMA and FITC-BSA (Figure 4d,e), the width and height of the nanolines have increased by ~45 and ~20 nm which both indicate a layer increase of ~20 nm. This shows a uniform attachment of FITC-BSA on the Au nanolines *via* electrostatic interaction.

Metal nanoparticles are potential building blocks for nanoelectronic devices, for example, using the Coulomb blockade effect.[33−35] A Coulomb blockade is normally visible at low temperatures for large particles.[36] By decreasing the metal island size down to 1−2 nm, Coulomb blockades can be observed at room temperature, which is a key issue for real-world applications of single electron devices.[35] However, to precisely position and integrate such small particles into functional devices is quite challenging. Previous efforts in this area have consisted primarily of lithographic patterning followed by random deposition[37,38] or the electrostatic[39] or magnetic[40] trapping of nanostructures. However, these approaches all feature challenges: they do not provide precise positioning, have difficulty in obtaining long distance, large areas, continuous connection, they require specific susceptibilities, have low throughput, and/or are not readily scalable.

In our work, the NAMIC approach was used to pattern ultrasmall Au NPs. The flow and the self-organization of the particles offer a better chance to achieve continuous NP patterns compared to other deposition methods. Additionally, the formation of the DTC bond between the Au NPs and the substrate achieves specific binding that can provide systems with a stable and uniform layer of NPs on the surface. Furthermore, the large areas fabricated with Au NP arrays allow the possibility to study the

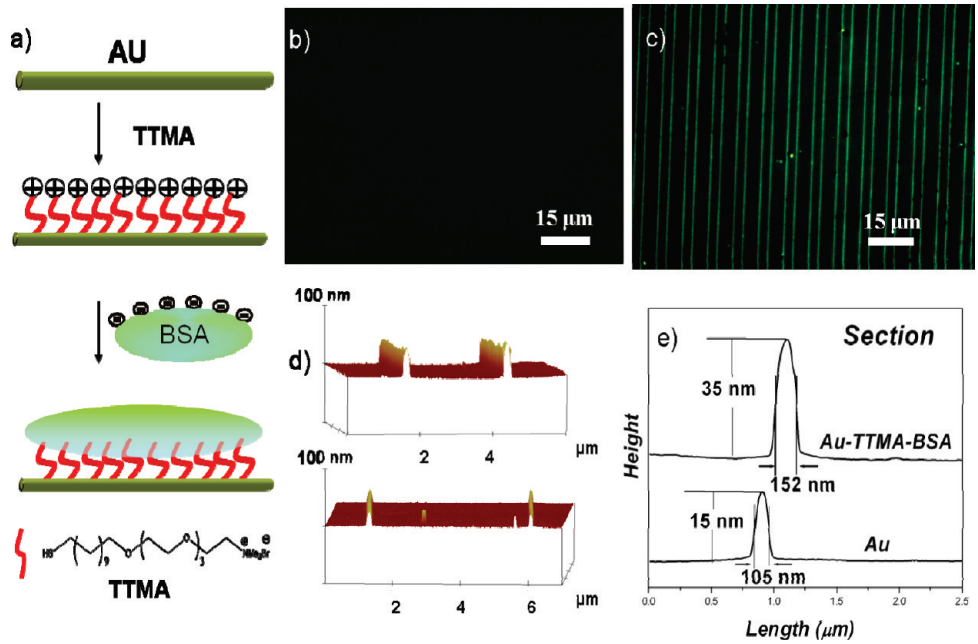

Figure 4. (a) Schematic illustration of the TTMA-functionalized Au nanolines and further deposition of FITC-BSA. Fluorescence micrographs (b,c), AFM 3D height images (d), and section analyses (e) of patterned Au nanolines before and after functionalization by the TTMA ligands and further electrostatic deposition of FITC-BSA.

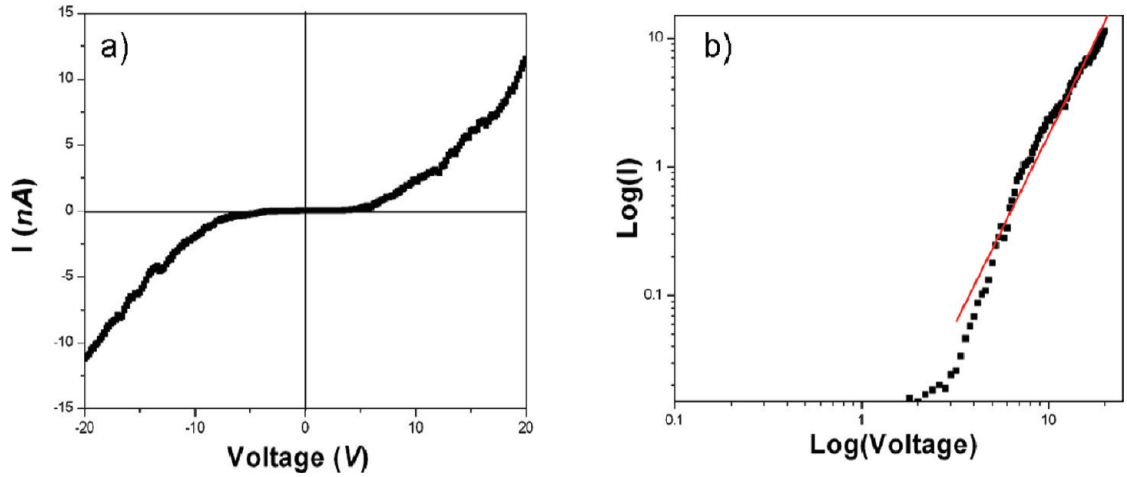

Figure 5. *I*−*V* characteristics (a) and the plot of log (*I*) *versus* log (*V*) (b) of the Au NP arrays fabricated by NAMIC using a 30 nm × 100 nm (*w* × *h*) mold at room temperature.

electrical properties of large arrays of particle structures instead of only one or a few particles lines as reported before.[37−40]

To measure the electrical properties of the patterned Au NP arrays, macroscopic conductive gold pads were fabricated on the Au NP arrays on SiO_2 substrates by thermal evaporation of gold and conventional lift-off procedures (see Supporting Information). Conductivity measurements were carried out by a two-probe method at room temperature. Figure 5 shows the *I*−*V* characteristics of the Au NP arrays fabricated by NAMIC using a 30 nm × 100 nm (*w* × *h*) mold on a SiO_2 substrate. Nonohmic current−voltage behavior was observed at applied voltages from −20 to 20 V (Figure 5a). The curves are strongly nonlinear, nearly symmetrical at $V = 0$, and have nonzero threshold voltages.

The NPs used in our study are composed of a gold core (~3.5 nm) encapsulated by a monolayer shell of the TOH ligand. This core−shell structure provides an intercore tunneling resistance, R_T, greater than the resistance quantum h/e^2 and should have a similar conducting behavior as in tunnel junction arrays.[41,42] As studied by Middleton and Wingreen,[43] electronic transport through an array of small metal particles separated by nanoscale gaps is determined by the interplay between the single-electron charging of an individual particle and the tunneling between adjacent particles. In the presence of a charge disorder due to quenched impurities in the insulating substrate under the array, this interplay leads to highly nonohmic current−voltage (*I*/*V*) characteristics. They predicted current suppression below a threshold voltage (V_t), while above this threshold the current follows a power law, $I \approx (V - V_i)^{\xi}$, with $\xi = 1$ in 1D and between $^5/_3$ and 2 in 2D.

In our case, as measured from SEM and AFM images (Figure 1e), the width and height of Au NP patterns are 40 and 18 nm, which correspond to around 5−6 Au NPs in parallel and 2−3 layers high, which can be considered as quasi-1D Au NP arrays. The *I*−*V* curve of the system should follow the power law which is predicted by Middleton and Wingreen.[43] When the data are plotted as log (*I*) *versus* log (*V*) (Figure 5b), a nearly straight line is obtained. From the slope and the intercept of this line, we infer that $\xi \approx 2.9$ and $V_t \approx 2.7$ V, which are comparable to some published data for a single layer or a short 1D array of Au NPs with similar dimensions.[15,20,42,44] This shows that our fabrication method represents a viable technique for creating large-area, continuous particle lines.

SUMMARY

A high-resolution soft lithographic technique to pattern Au, CdSe-based QDs, and FePt nanoparticles on surfaces has been developed. Nanomolding in capillaries (NAMIC) has been combined with dithiocarbamate (DTC) chemistry to immobilize NPs from solution to form arrays of uniform and stable sub-50 nm quasi-1D NP nanolines over large areas. Combined with the DTC chemistry, NAMIC shows the possibilities to create stable NP patterns, both in aqueous and organic solvents. The electrical properties of these patterned quasi-1D Au NP arrays have been studied, and these arrays are shown to be conducting and to have nonlinear *I*−*V* characteristics with nonzero threshold voltages consistent with Coulomb blockade behavior. The surface of the patterned Au NP arrays can be further functioned by thiol ligands, and bovine serum albumin (BSA) proteins were successfully adsorbed onto the NP arrays. These results show that the NAMIC method combined with surface chemistry is a facile and powerful approach for the patterning of colloidal nanostructures over large areas and represents a significant step toward the integration of bottom-up chemically prepared nanostructures with lithographically patterned nanostructures. It is also believed that these techniques can be applied as a valuable tool to fabricate nanoelectronic or biosensing devices.

MATERIALS AND METHODS

Materials. Imprint resist mr-I T85 was obtained from Micro Resist. The fluorescent isothiocyanate-labeled bovine serum albumin (FITC-BSA) and *N*-[3-(trimethoxysilyl)propyl]ethylenediamine (TPEDA) were purchased from Aldrich. All materials were used as received without further purification. Au NPs, FePt NPs, CdSe-based QDs, and TTMA (HS-C_{11}-tetra(ethylene glycol)NMe_3^+) ligand were prepared according to published results.[28] Silicon templates were fabricated by edge lithography followed by wet etching.[32] Two different sizes of nanoridges (30 nm and 100 nm wide, 100 nm high, separated by 4 μm) were used as imprint molds to fabricate the PDMS nanomold.

Composite Flat PDMS Substrates. Composite flat PDMS substrates were prepared by first casting the liquid prepolymer of the elastomer onto a polished Si wafer onto which an antiadhesion layer had been deposited. After degassing, a piece of cover glass (Menzel-Gläser BB015015A1 15 mm × 15 mm) which was cleaned by piranha solution (3:1 mixture of sulfuric acid and hydrogen peroxide. CAUTION! Piranha solutions should be handled with great care in open containers in a fume hood. Piranha is highly corrosive, toxic, and potentially explosive) was then put into the uncured mixture. The cover glass sank to the bottom of the PDMS liquid leaving a thin layer between the cover glass and the Si wafer. After curing at 60 °C for 8 h the stamp was peeled off from the Si wafer.

NIL Procedure. Before spin coating the resist, the composite PDMS substrate was treated by a short exposure of oxygen plasma (10 mTorr; 10 W; 20 sccm O_2; 15 s). This oxidation step increases the surface energy of the PDMS substrate to achieve a better film quality. A thin film of mr-I T85 solution was spin-coated onto the PDMS substrates, followed by a soft baking step for 2 min at 140 °C on a hot plate to form a 300 nm polymer layer. A stack of a composite PDMS substrate spin coated with mr-I T85 and a Si template coated with 1*H*,1*H*,2*H*,2*H*-perfluorodecyltrichlorosilane as an antiadhesion layer was inserted into a hydraulic press (Specac), and the temperature was raised to 140 °C. Then, 2 bar of pressure was applied to the system for 5 min. Upon cooling to 50 °C, the template was separated from the PDMS substrate.

Amine-Terminated Monolayer Preparation. Amine-terminated monolayers were prepared by immersing a cleaned silicon substrate into a 10 mM solution of TPEDA in ethanol for 12 h under N_2. The substrate was then removed from the solution and rinsed with CH_2Cl_2, ethanol, and CH_2Cl_2, followed by drying in a nitrogen flow.

NAMIC Procedure Combined with Dithiocarbamate (DTC) Bond Formation. Before NAMIC, a short oxygen plasma (10 mTorr; 10 W; 20 sccm O_2; 60 s) step was used to pretreat the PDMS nanomold surface to promote adhesion upon contacting the substrate. Thereafter, the nanomold was placed on the amine-modified substrate to form nanochannels. After the formation of the nanochannels, a drop of a NP solution containing 1:1 (v:v) mixture of a 200 nM aqueous solution of Au NPs at pH = 9.5 and a 100 mM CS_2 in ethanol solution was applied at the open ends of the nanochannels. Once the channels were filled completely, the solvent was allowed to evaporate at room temperature, and the NPs were precipitated out onto the substrate within the confinement of the channels. Once the solvent was completely evaporated, the PDMS nanomold was carefully peeled off from the substrate. Then the substrate was thoroughly rinsed with water and ethanol. Traces of residual T85 were observed on the substrate caused by the oxygen plasma pretreatment of the nanomolds, but these could be easily removed by oxygen plasma (20 mTorr; 20 W; 20 sccm O_2; 60 s).

Postdeposition of Fluorescent BSA. The patterned Au NP arrays on silicon substrates were immersed in a TTMA in ethanol solution (0.1 μM) for 8 h. The samples were then thoroughly washed with ethanol and dried in a nitrogen stream to achieve arrays of TTMA-functionalized Au nanolines (Au−TTMA). Subsequently, the substrates were incubated with fluorescent FITC-BSA (1 mg/mL) in water for electrostatic assembly. After 1 h, the substrates were washed with water several times and then dried in a nitrogen stream.

Measurements. AFM analyses were carried out with a NanoScope III (Veeco/Digital Instruments, Santa Barbara, CA, USA) multimode atomic force microscope equipped with a J-scanner, in tapping mode by using Si_3N_4 cantilevers (Nanoprobes, Veeco/Digital Instruments) with a nominal spring constant of about 0.32 N m^{-1}. AFM imaging was performed at ambient conditions. High-resolution SEM imaging was carried out with a JEOL Gemini 1550 FEG-SEM. Fluorescence microscopy was performed using an Olympus inverted research microscope IX71 equipped with a mercury burner U-RFL-T as light source and a digital camera Olympus DP70 (12.5 million-pixel cooled digital color camera) for image acquisition. Red emission light ($A > 590$ nm) was filtered using a U-MWG Olympus filter cube. Electrical measurements were carried out in a Suss MicroTec PM300 manual probe station with a standard Keithley 4200 semiconductor characterization system.

Acknowledgment. The authors gratefully acknowledge financial support from the Nanotechnology network in The Netherlands NanoNed (Project No. TMM. 7125) and from the MESA+ Institute for Nanotechnology (SRO Nanofabrication). V.R. and M.H.P. acknowledge support for an EFRC (DE-SC0001087) funded by DOE-BES. We are grateful to Mark Smithers for SEM measurements and to Sander Smits for help with the conductivity measurement setup. Wilfred van der Wiel is thanked for helpful discussions.

Supporting Information Available: AFM images of the Au−TOH NPs deposited on Si/SiO_2 by NAMIC without CS_2 added; lithography details for Au contact pads on Au NP arrays through a metal evaporation and lift-off process. This material is available free of charge *via* the Internet at http://pubs.acs.org.

REFERENCES AND NOTES

1. Eychmuller, A. Structure and Photophysics of Semiconductor Nanocrystals. *J. Phys. Chem. B* **2000**, *104*, 6514–6528.
2. Shenhar, R.; Norsten, T. B.; Rotello, V. M. Polymer-Mediated Nanoparticle Assembly: Structural Control and Applications. *Adv. Mater.* **2005**, *17*, 657–669.
3. Schmid, G.; Corain, B. Nanoparticulated Gold: Syntheses, Structures, Electronics, and Reactivities. *Eur. J. Inorg. Chem.* **2003**, 3081–3098.
4. Ghosh, S. K.; Pal, T. Interparticle Coupling Effect on the Surface Plasmon Resonance of Gold Nanoparticles: From Theory to Applications. *Chem. Rev.* **2007**, *107*, 4797–4862.
5. Shipway, A. N.; Katz, E.; Willner, I. Nanoparticle Arrays on Surfaces for Electronic, Optical, and Sensor Applications. *ChemPhysChem* **2000**, *1*, 18–52.
6. Ofir, Y.; Samanta, B.; Rotello, V. M. Polymer and Biopolymer Mediated Self-Assembly of Gold Nanoparticles. *Chem. Soc. Rev.* **2008**, *37*, 1814–1823.
7. Kralchevsky, P. A.; Denkov, N. D.; Paunov, V. N.; Velev, O. D.; Ivanov, I. B.; Yoshimura, H.; Nagayama, K. Formation of 2-Dimensional Colloid Crystals in Liquid-Films under the Action of Capillary Forces. *J. Phys.: Condens. Matter* **1994**, *6*, A395–A402.
8. Parthasarathy, R.; Lin, X. M.; Jaeger, H. M. Electronic Transport in Metal Nanocrystal Arrays: The Effect of Structural Disorder on Scaling Behavior. *Phys. Rev. Lett.* **2001**, *87*, 186807.
9. Morgan, N. Y.; Leatherdale, C. A.; Drndic, M.; Jarosz, M. V.; Kastner, M. A.; Bawendi, M. Electronic Transport in Films of Colloidal CdSe Nanocrystals. *Phys. Rev. B* **2002**, *66*, 075339.
10. Yu, D.; Wang, C. J.; Wehrenberg, B. L.; Guyot-Sionnest, P. Variable Range Hopping Conduction in Semiconductor Nanocrystal Solids. *Phys. Rev. lett.* **2004**, *92*, 216802.
11. Richardi, J. One-Dimensional Assemblies of Charged Nanoparticles in Water: A Simulation Study. *J. Chem. Phys.* **2009**, *130*, 044701.
12. Xu, K.; Qin, L. D.; Heath, J. R. The Crossover from Two Dimensions to One Dimension in Granular Electronic Materials. *Nat. Nanotechnol.* **2009**, *4*, 368–372.
13. Zhang, Y. X.; Zeng, H. C. Template-Free Parallel One-Dimensional Assembly of Gold Nanoparticles. *J. Phys. Chem. B* **2006**, *110*, 16812–16815.
14. Tang, Z. Y.; Kotov, N. A. One-Dimensional Assemblies of Nanoparticles: Preparation, Properties, and Promise. *Adv. Mater.* **2005**, *17*, 951–962.

15. Elteto, K.; Lin, X. M.; Jaeger, H. M. Electronic Transport in Quasi-One-Dimensional Arrays of Gold Nanocrystals. *Phys. Rev. B* **2005**, *71*, 205412.
16. Huang, J. X.; Tao, A. R.; Connor, S.; He, R. R.; Yang, P. D. A General Method for Assembling Single Colloidal Particle Lines. *Nano Lett.* **2006**, *6*, 524–529.
17. Dziomkina, N. V.; Vancso, G. J. Colloidal Crystal Assembly on Topologically Patterned Templates. *Soft Matter* **2005**, *1*, 265–279.
18. Niemeyer, C. M. Nanoparticles, Proteins, and Nucleic Acids: Biotechnology Meets Materials Science. *Angew. Chem., Int. Ed.* **2001**, *40*, 4128–4158.
19. Richter, J.; Mertig, M.; Pompe, W.; Monch, I.; Schackert, H. K. Construction of Highly Conductive Nanowires on a DNA Template. *Appl. Phys. Lett.* **2001**, *78*, 536–538.
20. Ancona, M. G.; Kooi, S. E.; Kruppa, W.; Snow, A. W.; Foos, E. E.; Whitman, L. J.; Park, D.; Shirey, L. Patterning of Narrow Au Nanocluster Lines Using V_2O_5 Nanowire Masks and Ion-Beam Milling. *Nano Lett.* **2003**, *3*, 135–138.
21. Westerlund, F.; Bjornholm, T. Directed Assembly of Gold Nanoparticles. *Curr. Opin. Colloid Interface Sci.* **2009**, *14*, 126–134.
22. Kouklin, N.; Menon, L.; Bandyopadhyay, S. Room-Temperature Single-Electron Charging in Electrochemically Synthesized Semiconductor Quantum Dot and Wire Array. *Appl. Phys. Lett.* **2002**, *80*, 1649–1651.
23. Cui, Y.; Bjork, M. T.; Liddle, J. A.; Sonnichsen, C.; Boussert, B.; Alivisatos, A. P. Integration of Colloidal Nanocrystals into Lithographically Patterned Devices. *Nano Lett.* **2004**, *4*, 1093–1098.
24. Kraus, T.; Malaquin, L.; Schmid, H.; Riess, W.; Spencer, N. D.; Wolf, H. Nanoparticle Printing with Single-Particle Resolution. *Nat. Nanotechnol.* **2007**, *2*, 570–576.
25. Cheng, J. Y.; Zhang, F.; Chuang, V. P.; Mayes, A. M.; Ross, C. A. Self-Assembled One-Dimensional Nanostructure Arrays. *Nano Lett.* **2006**, *6*, 2099–2103.
26. Xia, Y. N.; Whitesides, G. M. Soft Lithography. *Angew. Chem., Int. Ed.* **1998**, *37*, 550–575.
27. Duan, X. X.; Zhao, Y.; Berenschot, E.; Tas, N. R.; Reinhoudt, D. N.; Huskens, J. Large-Area Nanoscale Patterning of Functional Materials by Nanomolding in Capillaries. *Adv. Funct. Mater.* **2010**, *20*, 2519–2526.
28. Park, M. H.; Ofir, Y.; Samanta, B.; Rotello, V. M. Robust and Responsive Dendrimer−Gold Nanoparticle Nanocomposites *via* Dithiocarbamate Crosslinking. *Adv. Mater.* **2009**, *21*, 2323–2327.
29. Park, M. H.; Ofir, Y.; Samanta, B.; Arumugam, P.; Miranda, O. R.; Rotello, V. M. Nanoparticle Immobilization on Surfaces *via* Activatable Heterobifunctional Dithiocarbamate Bond Formation. *Adv. Mater.* **2008**, *20*, 4185–4188.
30. Park, M.-H.; Duan, X. X.; Ofir, Y.; Creran, B.; Patra, D.; Ling, X. Y.; Huskens, J.; Rotello, V. M. Chemically Directed Immobilization of Nanoparticles onto Gold Substrates for Orthogonal Assembly Using Dithiocarbamate Bond Formation. *ACS Appl. Mater. Interface* **2010**, *2*, 795–799.
31. Duan, X. X.; Zhao, Y. P.; Perl, A.; Berenschot, E.; Reinhoudt, D. N.; Huskens, J. High-Resolution Contact Printing with Chemically Patterned Flat Stamps Fabricated by Nanoimprint Lithography. *Adv. Mater.* **2009**, *21*, 2798–2802.
32. Zhao, Y.; Berenschot, E.; de Boer, M.; Jansen, H.; Tas, N.; Huskens, J.; Elwenspoek, M. Fabrication of a Silicon Oxide Stamp by Edge Lithography Reinforced with Silicon Nitride for Nanoimprint Lithography. *J. Micromech. Microeng.* **2008**, *18*, 064013.
33. Korotkov, A. N.; Chen, R. H.; Likharev, K. K. Possible Performance of Capacitively Coupled Single-Electron Transistors in Digital Circuits. *J. Appl. Phys.* **1995**, *78*, 2520–2530.
34. Feldheim, D. L.; Grabar, K. C.; Natan, M. J.; Mallouk, T. E. Electron Transfer in Self-Assembled Inorganic Polyelectrolyte/Metal Nanoparticle Heterostructures. *J. Am. Chem. Soc.* **1996**, *118*, 7640–7641.
35. Andres, R. P.; Bein, T.; Dorogi, M.; Feng, S.; Henderson, J. I.; Kubiak, C. P.; Mahoney, W.; Osifchin, R. G.; Reifenberger, R. "Coulomb Staircase" at Room Temperature in a Self-Assembled Molecular Nanostructure. *Science* **1996**, *272*, 1323–1325.
36. Teranishi, T. Fabrication and Electronic Properties of Gold Nanoparticle Superlattices. *C. R. Chim.* **2003**, *6*, 979–987.
37. Klein, D. L.; Roth, R.; Lim, A. K. L.; Alivisatos, A. P.; McEuen, P. L. A Single-Electron Transistor Made from a Cadmium Selenide Nanocrystal. *Nature* **1997**, *389*, 699–701.
38. Spatz, J. P.; Chan, V. Z. H.; Mossmer, S.; Kamm, F. M.; Plettl, A.; Ziemann, P.; Moller, M. A Combined Top-Down/Bottom-Up Approach to the Microscopic Localization of Metallic Nanodots. *Adv. Mater.* **2002**, *14*, 1827–1832.
39. Bezryadin, A.; Dekker, C.; Schmid, G. Electrostatic Trapping of Single Conducting Nanoparticles between Nanoelectrodes. *Appl. Phys. Lett.* **1997**, *71*, 1273–1275.
40. Lee, C. S.; Lee, H.; Westervelt, R. M. Microelectromagnets for the Control of Magnetic Nanoparticles. *Appl. Phys. Lett.* **2001**, *79*, 3308–3310.
41. Alivisatos, A. P.; Johnsson, K. P.; Peng, X. G.; Wilson, T. E.; Loweth, C. J.; Bruchez, M. P.; Schultz, P. G. Organization of 'Nanocrystal Molecules' Using DNA. *Nature* **1996**, *382*, 609–611.
42. Clarke, L.; Wybourne, M. N.; Yan, M. D.; Cai, S. X.; Keana, J. F. W. Transport in Gold Cluster Structures Defined by Electron-Beam Lithography. *Appl. Phys. Lett.* **1997**, *71*, 617–619.
43. Middleton, A. A.; Wingreen, N. S. Collective Transport in Arrays of Small Metallic Dots. *Phys. Rev. Lett.* **1993**, *71*, 3198–3201.
44. Ancona, M. G.; Kruppa, W.; Rendell, R. W.; Snow, A. W.; Park, D.; Boos, J. B. Coulomb Blockade in Single-Layer Au Nanocluster Films. *Phys. Rev. B* **2001**, *64*, 033408.